Giant Ferroelectric Polarization in Ultrathin Ferroelectrics via Boundary-Condition Engineering

Lin Xie, Linze Li, Colin A. Heikes, Yi Zhang, Zijian Hong, Peng Gao, Christopher T. Nelson, Fei Xue, Emmanouil Kioupakis, Longqing Chen, Darrel G. Schlom, Peng Wang, and Xiaoqing Pan*

Tailoring and enhancing the functional properties of materials at reduced dimension is critical for continuous advancement of modern electronic devices. Here, the discovery of local surface induced giant spontaneous polarization in ultrathin BiFeO$_3$ ferroelectric films is reported. Using aberration-corrected scanning transmission electron microscopy, it is found that the spontaneous polarization in a 2 nm-thick ultrathin BiFeO$_3$ film is abnormally increased up to ≈90–100 µC cm^{-2} in the out-of-plane direction and a peculiar rumpled nanodomain structure with very large variation in c/a ratios, which is analogous to morphotropic phase boundaries (MPBs), is formed. By a combination of density functional theory and phase-field calculations, it is shown that it is the unique single atomic Bi$_2$O$_{3-x}$ layer at the surface that leads to the enhanced polarization and appearance of the MPB-like nanodomain structure. This finding clearly demonstrates a novel route to the enhanced functional properties in the material system with reduced dimension via engineering the surface boundary conditions.

The integration of ferroelectric thin films into electronic devices has led to an upsurge of interest in exploring novel devices with exotic physical properties, owing to the multitude of functionality of ferroelectrics.[1–3] A number of applications, e.g.,

Dr. L. Xie, Dr. L. Z. Li, Dr. Y. Zhang, Prof. X. Q. Pan
Department of Chemical Engineering and Materials Science
University of California Irvine
Irvine, CA 92697, USA
E-mail: xiaoqinp@uci.edu
Dr. L. Xie, Prof. P. Wang, Prof. X. Q. Pan
National Laboratory of Solid State Microstructures
and College of Engineering and Applied Sciences
Nanjing University
Nanjing, Jiangsu 210093, P. R. China
Dr. C. A. Heikes, Prof. D. G. Schlom
Department of Materials Science and Engineering
Cornell University
Ithaca, NY 14850, USA
Dr. Z. J. Hong, Dr. F. Xue, Prof. L.-Q. Chen
Department of Materials Science and Engineering
Pennsylvania State University
State College, PA 16802, USA
Dr. P. Gao, Dr. C. T. Nelson, Prof. E. Kioupakis
Department of Materials Science and Engineering
University of Michigan
Ann Arbor, MI 48105, USA

high-density nonvolatile random access memories[4] and prototype devices in electronics, optoelectronics, and electromechanics, have been proposed based on the coupling between the ferroelectric polarization and other functional properties, i.e., mechanical, optical, and magnetic properties of ferroelectric materials.[2,5–7] However, as the size of the device with ferroelectrics is reduced to the scale required for practical industrial semiconductor devices, this development is challenged by the long-standing issue concerning the "dead layer" or size scaling effect, where ferroelectric polarization in films with a thickness down to a few nanometers is hampered due to the strong depolarizing electric field, which arises from the incomplete screening at the surface or interface.[8–10] On the other hand, several experimental studies have indicated that the spontaneous polarization in a ferroelectric thin film can be retained down to the thickness of only several unitcells,[7,11–14] but with reduced transition temperature[11] and polarization.[13] Therefore, given the thriving practical industrial applications of nanoelectronic devices, it is of great importance to pursue enhanced ferroelectric properties at the reduced dimension. Using atomistic simulations, it has been demonstrated that an overall enhancement of ferroelectricity can be produced in ultrathin ferroelectric capacitors by controlling the chemical environments at the metal/oxide interfaces.[15] Recent experimental work suggested that a reduction in size to a scale of a few nanometers can lead to the emergence of weak room-temperature ferroelectricity in an otherwise nonferroelectric SrTiO$_3$ film, a result of electrically induced alignment of polar nanoregions due to Sr vacancies.[16] However, a direct experimental observation of enhanced polarizations at reduced dimensions in common ferroelectrics has not yet been deterministically identified. In this study, a 2 nm thick ultrathin BFO film was prepared, and its structural properties were investigated to demonstrate that a prominent enhancement of ferroelectric polarization and the formation of MPB-like domain structure can be achieved by changing the surface boundary condition through single atomic Bi$_2$O$_{3-x}$ layers.

The films studied here are epitaxially grown on TbScO$_3$ (TSO) $(1\bar{1}0)_O$ substrates by molecular-beam epitaxy; the growth direction for BFO is [001]$_{PC}$ (the subscripts O and PC stand
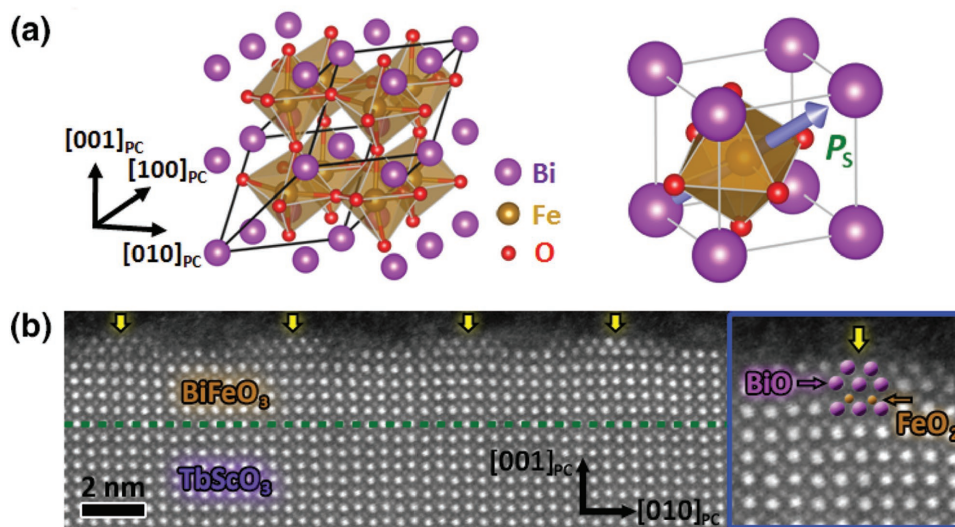
**ADVANCED
SCIENCE NEWS**

www.advancedsciencenews.com

**ADVANCED
MATERIALS**

www.advmat.de

Figure 1. The atomic structure of $BiFeO_3$ and an STEM HAADF image of a 2 nm thick $BiFeO_3/TbScO_3$ $(1\bar{1}0)_O$ film. a) Schematic structure of the rhombohedral phase of $BiFeO_3$. b) Cross-sectional STEM HAADF image of a 2 nm thick $BiFeO_3/TbScO_3$ film viewed along the $[100]_{PC}$ zone axis, where the interface is indicated by the green dashed line. The yellow arrows indicate the unique single atomic layers on the surface. For a better view of the surface structure, see the inset for a magnified image.

for orthorhombic and pseudocubic indices, respectively). At ambient conditions, a BFO/TSO $(1\bar{1}0)_O$ thin film is typically of rhombohedral (*R*) phase, with its spontaneous polarization $\mathbf{P}_S$ (≈ 90 µC cm^{-2}) pointing in one of the symmetrically equivalent $<111>_{PC}$ directions (**Figure 1**a).[17,18] The ultrathin film was characterized by scanning transmission electron microscopy (STEM) high-angle annular dark field (HAADF) imaging and Figure 1b shows the atomic-resolution image viewed along the $[100]_{PC}$ direction. Note that the film has two remarkable structural features. First, unlike conventional epitaxial thin films with flat surface, the film is not homogeneous in terms of its out-of-plane lattice, but characterized by a peculiar periodic rumpled structure. This rumpling essentially takes the form of periodic lattice dilations along the film's growth direction, i.e., $[001]_{PC}$. Second, as indicated by the yellow arrows, there also exist unique structures on the film's surface. These particular surface structures are discontinuous and only one single atomic layer in thickness (see the inset of Figure 1b for a better view of the surface structure). Their reduced image contrast with respect to the film is probably due to the discontinuous distribution of these monolayers along the beam direction as well (see Supporting Information for details). As shall be shown below, these two structural features are closely associated with each other and give rise to a large enhancement in the ferroelectric polarizations.

The rumpling structure and ferroelectricity of the film are characterized by measuring the relative displacements of *B*-site Fe atoms $\mathbf{D}_{FB}$ with respect to the center of four surrounding *A*-site Bi atoms.[19,20] Local ferroelectric polarization $\mathbf{P}_S$ is related to $\mathbf{D}_{FB}$ as $\mathbf{P}_S \propto -\mathbf{D}_{FB}$ since, in general, the relative displacement of the Fe atom is in the opposite direction of the polarization. **Figure 2**a shows the map of the local Fe displacements and clearly illustrates the local ferroelectric polarization and domain structure. Unlike the conventional *R*-phase BFO (shown in Figure 1a), the domain structure of the film is similar to those

expected for the mixture of tetragonal (*T*) phase and *R*-phase ferroelectrics and closely resemble the "morphotropic phase boundary" found in $Pb(Zr_{0.5}Ti_{0.5})O_3$.[21] Here the "morphotropic" term is used to refer to the different symmetry of the domains. In the following text, we will denote the domains with large out-of-plane component as *c*-type domains, while those with attenuated polarization are denoted as *a*-type domains. The alternating *c*-/*a*-type domain structures and lattice dilations can be seen more clearly in the maps of the out-of-plane displacement $-D_{FB}^{(z)}$ (Figure 2b) and the c/a ratios (Figure 2c). Note that there is a perfect one-to-one match between the domains and the appearance of the surface monolayer, where the single atomic layer appears exclusively on top of the *c*-type domains.

Careful analysis of the c/a ratios, $|\mathbf{D}_{FB}|$ and $-D_{FB}^{(z)}$ of these two types of domains is given in Figure 2d–f. At the interface, the c/a ratios of both *c*-type and *a*-type domains are close to the bulk value (≈ 1.0). The c/a ratio of *c*-type domains monotonically increases from the interface to the surface, while that of *a*-type domains seems relatively uniform through the film. At the top surface, the c/a ratio of *c*-type domains reaches up to a value of ≈ 1.15. Meanwhile, the ferroelectric displacements $|\mathbf{D}_{FB}|$ and $-D_{FB}^{(z)}$ of *c*-type domains behave in a similar manner to their c/a ratios. At the interface, $|\mathbf{D}_{FB}|$ of *c*-type domains ($\approx 0.28 \pm 0.05$ Å) is comparable to the bulk value ≈ 0.33 Å. At the top surface of the film, $|\mathbf{D}_{FB}|$ increases dramatically to a value of $\approx 0.5 \pm 0.08$ Å, nearly 30% greater than the bulk value. The corresponding $-D_{FB}^{(z)}$ is also markedly enhanced to $\approx 0.4 \pm 0.02$ Å. To estimate the resulting polarization, we assume that $\mathbf{P}_S$ is proportional to $|\mathbf{D}_{FB}|$[19] and given a polarization of ≈ 90 µC cm^{-2} for $|\mathbf{D}_{FB}| = 0.33$ Å, a giant polarization of ≈ 136 µC cm^{-2} is obtained for $|\mathbf{D}_{FB}| = 0.5$ Å. Similarly, the out-of-plane polarization is estimated to be ≈ 109 µC cm^{-2} for $-D_{FB}^{(z)} = 0.4$ Å. In comparison, the out-of-plane polarization of *a*-type domains is significantly suppressed, and $-D_{FB}^{(z)}$ is only about ≈ 0.05–0.13 (± 0.07) Å, much smaller than its bulk counterpart.

ADVANCED
SCIENCE NEWS
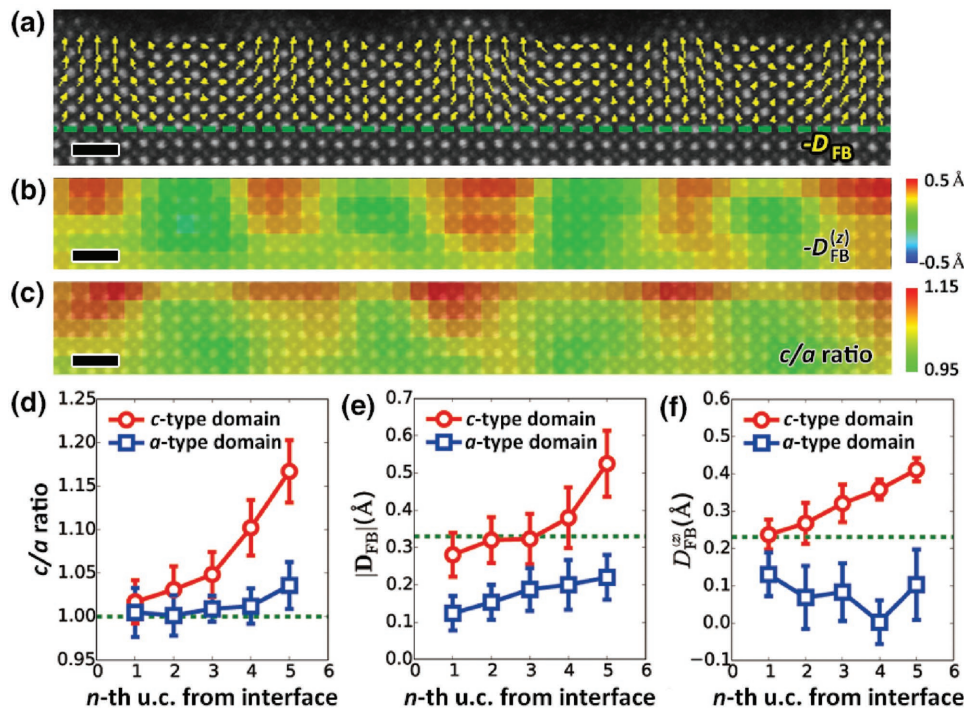www.advancedsciencenews.com

ADVANCED
MATERIALS
www.advmat.de

Figure 2. Maps of the ferroelectric polarization and c/a ratio of the 2 nm thick BiFeO$_3$ film. a) $-D_{FB}$ map, b) $-D_{FB}^{(z)}$ map, c) c/a ratio map of the film. The scale bars in (a)–(c) are 1 nm. d) c/a ratio as a function of distance from the interface, e,f) $|D_{FB}|$ (e) and $-D_{FB}^{(z)}$ (f) of c-/a-type domains. The green dashed lines in (d)–(f) indicate the c/a ratio, $|D_{FB}|$ and $-D_{FB}^{(z)}$ of bulk BiFeO$_3$, respectively.

Using the same approximation, the polarization is estimated to be only about ≈14–35 (±19) μC cm^{-2}. While the suppression of polarization due to the presence of a depolarizing field is expected in ultrathin ferroelectric films, an anomalous polarization enhancement up to ≈136 μC cm^{-2} is very surprising. This value is even comparable to that of super-tetragonal BFO films, in which a polarization up to ≈150 μC cm^{-2} can be induced by a large compressive epitaxial strain.[22] More importantly, according to conventional understanding of ferroelectric polarization in ultrathin films, its spontaneous polarization is expected to be substantially suppressed by the surface and the depolarizing field.[8,9] Our results for the first time clearly demonstrate that ferroelectricity can be prominently enhanced and novel MPB-like domain structure can form in an ultrathin ferroelectric film by changing the surface condition.

The driving force of the as-observed enhanced polarization, as well as the large lattice dilations, cannot be simply explained by the epitaxial strain applied by the substrate (the lattice mismatch between BFO and TSO is <0.14%)[19,23] and should have other explanation. The one-to-one correspondence between the appearance of the c-type domains with enhanced polarization and the surface monolayers might be a possible mechanism. In fact, it was found that a parasitic bismuth compound in BFO could lead to a tetragonal BFO phase with a giant c/a ratio,[24] which suggest that the abnormally enhanced polarization and c/a ratios might be related to the surface monolayers. In order to gain deeper insights into the underlying physics of the enhanced ferroelectric and the surface monolayer, we carry out further chemical analysis of the surface structure. As is shown in the inset of Figure 1b, the single atomic layer does

not comply with the $ABAB$ (A – BiO plane, B – FeO$_2$ plane) stacking order of BFO. Instead, the atoms are shifted with respect to the lower BiO planes and result in a characteristic zigzag-like structure. The chemical composition of the surface layers was investigated via electron energy-loss spectroscopy (EELS) line scans from the substrate to the surface (see the Experimental Section for details of EELS experiments). Six individual spectra, five for the BFO film, and one for the single atomic surface layer, are extracted from the line scan profile and the processed spectra are displayed in **Figure 3**. While the lower five spectra of the BFO film all show the elemental O K (≈530 eV) and Fe L$_{2,3}$ (≈708 eV) energy-loss peaks, the surface layers are deficient in Fe. Meanwhile, the proportion of O changes much less. Direct evidence of Bi in the surface monolayer is difficult to obtain straightforwardly from EELS due to its extremely high energy loss (≈2580 eV). But provided that the HAADF image contrast of the surface layers is similar to that of the film, it is strongly inferred that the surface layer is primarily a compound of Bi and O, and the most probable candidate is nonstoichiometric Bi$_2$O$_{3-x}$. In fact, Bi$_2$O$_{3-x}$ has a relatively small lattice mismatch with BFO[25] and its structure (Figure S1, Supporting Information) is also in reasonably good agreement with the characteristic zigzag-like structure discovered in the HAADF images. The formation of such surface monolayers is possibly due to certain surface reconstruction or relaxation processes.[26,27] Another plausible explanation is that these atomic layers originate from an outward migration of the lower BiO planes due to the volatility of Bi. It should also be noted that similar structure with elongated lattice parameters occur in the form of antiphase boundary in doped BFO,[28,29]
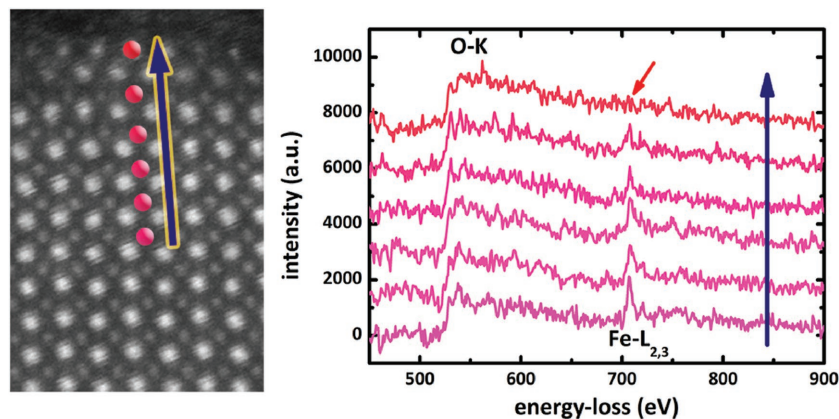
**ADVANCED
SCIENCE NEWS**

www.advancedsciencenews.com

**ADVANCED
MATERIALS**

www.advmat.de

Figure 3. Line scan profile of Fe $L_{2,3}$ and O K energy-loss spectra. The position of each EELS spectrum (from bottom to top) is indicated by the circles in the left panel and the corresponding spectrum is shown in the right panel from bottom to top. As is indicated by the red arrow, the energy-loss peak of Fe $L_{2,3}$ (≈708 eV) vanishes at the surface layer, while that of O K changes much less through the film.

which suggests that these surface monolayers might be nucleation sites during growth. If more FeO_2 is added, this transient state would become proper BFO. In fact, such an implication is supported by a sequence of films grown at different thickness, in which the same surface structure can be observed (see Supporting Information for the discussions of the surface structure, Figure S2 and S3, and experimental results of films with different thickness, Figure S4 and S5). Nonetheless, these structures are directly associated with the c-type domains and possibly a dominant factor in the enhanced ferroelectricity.

DFT calculations were carried out to corroborate the proposed surface enhanced polarization mechanism. In the calculation, a single Bi_2O_3 layer was placed on top of BFO and a full structural relaxation was performed (see Supporting Information for details of calculation). **Figure 4**a displays the atomic structure after the relaxation, and the lattice dilation can be readily observed at the top BFO layer. The calculated c/a ratio

and $|D_{FB}|$ are summarized in Figure 4b and they match the experimental values very well. First, the c/a ratio increases monotonically along the $[001]_{PC}$ direction, starting from ≈1.0 at the interface and reaching a value of ≈1.2 at the surface. Second, the calculated $|D_{FB}|$ at the interface is ≈0.33 Å and increases substantially to a value of ≈0.58 Å at the top surface. Local polarization was then calculated from the relaxed structure. According to modern theory of polarization,[30,31] the polarization $\mathbf{P}_i$ of unit cell i is:[32]

$$\mathbf{P}_i = \frac{1}{\Omega_i} \sum_j Z^*_{i,j} \delta \mathbf{u}_{i,j} \tag{1}$$

where Ω_i is the volume of unit cell i and $Z^*_{i,j}$ and $\delta \mathbf{u}_{i,j}$ are the Born effective charge tensor, and relative displacement of jth atom, respectively. The calculated total polarization, including the in-plane and out-of-plane components, are shown in Figure 4c. Near the BFO/TSO interface, $|\mathbf{P}_i|$ is close to the bulk value ≈90 μC cm^{-2}. At the Bi_2O_3/BFO interface, $|\mathbf{P}_i|$ reaches a value as large as ≈140 μC cm^{-2} and matches the experimental result (≈136 μC cm^{-2}) very well. The out-of-plane polarization (≈86 μC cm^{-2}) is also in reasonable agreement with the experiment (≈109 μC cm^{-2}). It is worthwhile to point out that even the out-of-plane polarization alone is already comparable to the total polarization of bulk BFO and indicates a better ferroelectric property. The strong coupling between the surface monolayer and the polarization of BFO can be attributed to the break of local symmetry and the change of the ionic charge of the Bi atoms at the surface. Table S1 and Figure S6 (Supporting Information) summarize the Bader charge analysis[33] and layer-resolved density of states of Bi and O atoms for our simulated structure. Our results show that, although the ionic charge of Bi in BFO is +1.87 (close to the +2 oxidation state), its
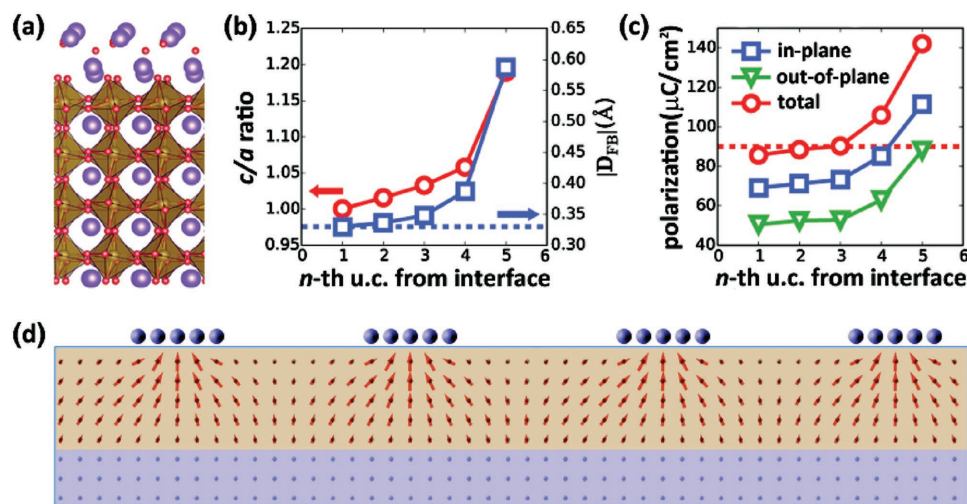

Figure 4. DFT and phase-field calculation results of ultrathin $BiFeO_3$ film with a single atomic Bi_2O_3 layer on the surface. a) Atomic structure after structural relaxation, b) c/a ratio, $|D_{FB}|$, and c) ferroelectric polarization by DFT. The blue and red dashed lines indicate $|D_{FB}|$ and total polarization of bulk $BiFeO_3$, respectively. d) Phase-field simulation results.

**ADVANCED
SCIENCE NEWS**
www.advancedsciencenews.com

**ADVANCED
MATERIALS**
www.advmat.de

value at the Bi_2O_3/BFO interface reduces to +1.64 and down to only +1.27 in Bi_2O_3 layer, indicating that the nominally empty Bi $6p$ orbitals become occupied near the surface (see Supporting Information for further details). The lower ionic charge of Bi atoms in Bi_2O_3 weakens the attraction between Bi and O atoms compared to BFO and increases their bond length. Consequently, the imbalance between the weaker Bi–O bond in the vicinity of the surface and the comparatively stronger bond in BFO leads to a strong dipole field, which effectively counteracts the depolarizing field and causes the enhancement in polarization.

The formation of the rumpling *c*-/*a*-type MPB-like domain structure can be explained by incorporating the surface single layer structures into phase-field simulations (see Supporting Information for details). The interaction between the surface layer and BFO film was modeled by applying an effective built-in potential on the surface with the surface monolayer. The result is shown in Figure 4d, which qualitatively reproduces the rumpling *c*-type/*a*-type domain structure. The simulated c/a ratio and $|\mathbf{P}_i|$ of *c*-type domains are consistent with both experiments and DFT calculations as well (see Figure S7 and S8, Supporting Information). Without such surface layer, the polarization in this ultrathin film would otherwise be substantially suppressed, due to the depolarizing field as well as the surface effect. This is clearly observed at the bottom layers of the film from both phase-field simulation and the experimental data, where the polarization is less affected by the surface layer. Near the surface layers, the polarization is mainly upward, indicating a super tetragonal-like phase. Meanwhile, a polarization component normal to the mapping plane is also found in the simulation and consistent with the strain induced super tetragonal phase.[34] In summary, our DFT and phase-field simulations fully reproduce the key experimental results and reveal a novel polarization enhancing scenario, where a potential enhancement of ultrathin films' ferroelectricity can be realized via the introduction of specific surface structures.

We remark that the unique Bi_2O_{3-x} monolayer observed by our STEM experiments and the enhanced polarization is nontrivial and it might be ubiquitous for BFO films. As a matter of fact, the same surface structures are also observed in 5 and 20 nm thick BFO films. With the increase of thickness, their effects become less prominent and hence these films exhibit the conventional 109° domain structures of *R*-phase BFO (see Figure S4 and S5, Supporting Information). Nevertheless, the ferroelectricity in the vicinity of the surface layers is still affected. For example, Figure S4a (Supporting Information) displays a map of the c/a ratio and $-D_{FB}^{(z)}$ for a 5 nm BFO film. Similar to the ultrathin 2 nm film, a substantial increase of $-D_{FB}^{(z)}$ up to ≈0.48 Å near the surface is found. Similar phenomena have also been reported in BFO/$La_{0.7}Sr_{0.3}MnO_3$/$SrTiO_3$ thin films by Kim et al.[35] Using STEM, they discovered a sudden increase of displacement (≈90–100%) and lattice spacing (≈10%) at the surface and these structural anomalies are interpreted as surface dielectric dead layers. The unique MPB-like nanodomain structure and the very large c/a ratio (≈1.2) of the *c*-type domains suggest a possibly very good piezoelectric response property of the ultrathin film because the domain structure is similar to MPB[36] and a change of the overall polarization of the thin film could lead to large strain variations. Therefore, it might

be useful to develop high-performance ultrathin piezoelectric response nanodevices. However, in order to exploit these structures to obtain well-controlled enhanced polarization and MPB-like domain structure in the ferroelectric thin films, a very fine control of the surface chemistry is mandatory. A possible route is to combine molecular beam epitaxy (MBE) growth together with electron lithography. Furthermore, it is also worthwhile to note that whether similar polarization enhancement mechanism could be applied to other perovskite ferroelectric materials, e.g., the classical $BaTiO_3$, $Pb(Ti_{1-x}Zr_x)O_3$ systems at the reduced dimension is still an open question and follow-up work is still undergoing. We note that recent work by Fan et al.[37] showed that by doping BFO film with Ga, a super-tetragonal-like structure with largely enhanced polarization could be stabilized regardless of film thickness. This finding, along side with our results, could possibly give rise to material systems of far more superior performance.

In conclusion, our combined experimental and theoretical studies clearly demonstrate how an enhancement of ferroelectricity can be achieved in ultrathin ferroelectric films through the engineering of its surface. This is nontrivial because surface relaxation, reconstruction, and defects are very common in a variety of ferroelectric oxides.[38–40] The change of the surface structure will not only introduce lattice disorder and coordination distortion, but also give rise to long-range electrical dipole interactions because of the nature of ionic crystals. As a consequence, instead of being confined only at the surface, unexpected behaviors permeating throughout the whole film could be introduced. For example, a reversible switching of ferroelectric domains can be achieved by controlling the surface chemical potential.[41] In our case, the surface monolayer plays a similar role by introducing effective polarizing fields and leads to the unexpected giant polarizations and MPB-like nanodomains with large variations in c/a ratios. Our results demonstrate that novel or better physical properties can be exploited and explored by modifying the boundary condition of an ultrathin ferroelectric film's surface. These findings offer a new dimension and route to designing thin film structures and tailoring its properties by means of precise control of local ferroelectricity through the engineering of boundary conditions.

Experimental Section

Materials Synthesis and Characterization: The $BiFeO_3$ films were grown on single crystal $(1\bar{1}0)_O$ $TbScO_3$ substrate by reactive-MBE. The 2 nm thick $BiFeO_3$ layer was deposited at a substrate temperature of 625 °C in distilled ozone (≈80% ozone) at a partial pressure of 1×10^{-6} Torr. This window was determined for the estimated elemental fluxes of ≈2 × 10^{13} at cm^{-2} s^{-1} for Fe and ≈1 × 10^{13} at cm^{-2} s^{-1} for Bi as measured on a quartz crystal monitor prior to growth. The 5 nm films and 20 nm films were grown in a similar fashion with a growth temperature determined in the same manner prior to their growth. Cross-sectional transmission electron microscopy samples were prepared by mechanical polishing followed by argon ion milling. STEM HAADF and EELS experiments were carried out on an FEI Titan 80–300 microscope equipped with double aberration correctors at 300 kV. The accelerating voltage, convergence angle of the incident electrons, and the collection angle for HAADF imaging are 300 kV, 29 mrad, and 79–200 mrad, respectively. EELS experiments were performed with the convergence angle, the collection angle, and energy dispersion 22 mrad, 36 mrad, and 1 eV per channel,

**ADVANCED
SCIENCE NEWS**

www.advancedsciencenews.com

**ADVANCED
MATERIALS**

www.advmat.de

respectively. For each pixel, a dwell time of 0.1 s was used to acquire the EEL spectra.

Conflict of Interest

The authors declare no conflict of interest.

[1]   N. A. Spaldin, M. Fiebig, *Science* **2005**, *309*, 391.
[2]   M. Dawber, K. M. Rabe, J. F. Scott, *Rev. Mod. Phys.* **2005**, *77*, 1083.
[3]   R. Ramesh, N. A. Spaldin, *Nat. Mater.* **2007**, *6*, 21.
[4]   J. F. Scott, *Ferroelectric Memories*, Springer-Verlag, Berlin, Germany **2000**.
[5]   A. Gruverman, A. Kholkin, *Rep. Prog. Phys.* **2006**, *69*, 2443.
[6]   N. Setter, D. Damjanovic, L. Eng, G. Fox, S. Gevorgian, S. Hong, A. Kingon, H. Kohlstedt, N. Y. Park, G. B. Stephenson, I. Stolitchnov, A. K. Tagantsev, D. V. Taylor, T. Yamada, S. Streiffer, *J. Appl. Phys.* **2006**, *100*, 051606.
[7]   Z. Wen, C. Li, D. Wu, A. Li, N. Ming, *Nat. Mater.* **2013**, *12*, 617.
[8]   M. E. Lines, A. M. Glass, *Principles and Applications of Ferroelectrics and Related Materials*, Oxford University Press, Oxford, UK **2001**.
[9]   D. J. Kim, J. Y. Jo, Y. S. Kim, Y. J. Chang, J. S. Lee, J.-G. Yoon, T. K. Song, T. W. Noh, *Phys. Rev. Lett.* **2005**, *95*, 237602.
[10] A. Petraru, H. Kohlstedt, U. Poppe, R. Waser, A. Solbach, U. Klemradt, J. Schubert, W. Zander, N. A. Pertsev, *Appl. Phys. Lett.* **2008**, *93*, 072902.
[11] D. D. Fong, G. B. Stephenson, S. K. Streiffer, J. A. Eastman, O. Auciello, P. H. Fuoss, C. Thompson, *Science* **2004**, *304*, 1650.
[12] H. Béa, S. Fusil, K. Bouzehouane, M. Bibes, M. Sirena, G. Herranz, E. Jacquet, J.-P. Contour, A. Barthélémy, *Jpn. J. Appl. Phys.* **2006**, *45*, L187.
[13] L. Despont, C. Koitzsch, F. Clerc, M. G. Garnier, P. Aebi, C. Lichtensteiger, J.-M. Triscone, F. J. Garcia de Abajo, E. Bousquet, P. Ghosez, *Phys. Rev. B* **2006**, *73*, 094110.
[14] H. Yamada, V. Garcia, S. Fusil, S. Boyn, M. Marinova, A. Gloter, S. Xavier, J. Grollier, E. Jacquet, C. Carrétéro, C. Deranlot, M. Bibes, A. Barthélémy, *ACS Nano* **2013**, *7*, 5385.
[15] M. Stengel, D. Vanderbilt, N. A. Spaldin, *Nat. Mater.* **2009**, *8*, 392.
[16] D. Lee, H. Lu, Y. Gu, S.-Y. Choi, S.-D. Li, S. Ryu, T. R. Paudel, K. Song, E. Mikheev, S. Lee, S. Stemmer, D. A. Tenne, S. H. Oh, E. Y. Tsymbal, X. Wu, L.-Q. Chen, A. Gruverman, C. B. Eom, *Science* **2015**, *349*, 1314.
[17] G. Catalan, J. F. Scott, *Adv. Mater.* **2009**, *21*, 2463.
[18] Y.-H. Chu, L. W. Martin, M. B. Holcomb, R. Ramesh, *Mater. Today* **2007**, *10*, 16.
[19] C. T. Nelson, B. Winchester, Y. Zhang, S.-J. Kim, A. Melville, C. Adamo, C. M. Folkman, S.-H. Baek, C.-B. Eom, D. G. Schlom, L.-Q. Chen, X. Pan, *Nano Lett.* **2011**, *11*, 828.
[20] C. T. Nelson, P. Gao, J. R. Jokisaari, C. Heikes, C. Adamo, A. Melville, S.-H. Baek, C. M. Folkman, B. Winchester, Y. Gu, Y. Liu, K. Zhang, E. Wang, J. Li, L.-Q. Chen, C.-B. Eom, D. G. Schlom, X. Pan, *Science* **2011**, *334*, 968.
[21] L. A. Schmitt, K. A. Schönau, R. Theissmann, H. Fuess, H. Kungl, M. J. Hoffmann, *J. Appl. Phys.* **2007**, *101*, 251911.
[22] R. J. Zeches, M. D. Rossell, J. X. Zhang, A. J. Hatt, Q. He, C.-H. Yang, A. Kumar, C. H. Wang, A. Melville, C. Adamo, G. Sheng, Y.-H. Chu, J. F. Ihlefeld, R. Erni, C. Ederer, V. Gopalan, L. Q. Chen, D. G. Schlom, N. A. Spaldin, L. W. Martin, R. Ramesh, *Science* **2009**, *326*, 977.
[23] C. M. Folkman, S. H. Baek, H. W. Jang, C. B. Eom, C. T. Nelson, X. Q. Pan, Y. L. Li, L. Q. Chen, A. Kumar, V. Gopalan, S. K. Streiffer, *Appl. Phys. Lett.* **2009**, *94*, 251911.
[24] H. Liu, P. Yang, K. Yao, K. P. Ong, P. Wu, J. Wang, *Adv. Funct. Mater.* **2012**, *22*, 937.
[25] S. Hull, S. T. Norberg, M. G. Tucker, S. G. Eriksson, C. E. Mohn, S. Stolen, *Dalton Trans.* **2009**, *40*, 8737.
[26] X. Martí, P. Ferrer, J. Herrero-Albillos, J. Narvaez, V. Holy, N. Barrett, M. Alexe, G. Catalan, *Phys. Rev. Lett.* **2011**, *106*, 236101.
[27] R. Jarrier, X. Marti, J. Herrero-Albillos, P. Ferrer, R. Haumont, P. Gemeiner, G. Geneste, P. Berthet, T. Schülli, P. Cevc, R. Blinc, S. S. Wong, T.-J. Park, M. Alexe, M. A. Carpenter, J. F. Scott, G. Catalan, B. Dkhil, *Phys. Rev. B* **2012**, *85*, 184104.
[28] I. MacLaren, L. Wang, O. Morris, A. Craven, R. Stamps, *APL Mater.* **2013**, *1*, 021102.
[29] I. MacLaren, B. Sala, S. M. L. Andersson, T. J. Pennycook, J. Xiong, Q. X. Jia, E.-M. Choi, J. L. MacManus-Driscoll, *Nanoscale Res. Lett.* **2015**, *10*, 407.
[30] R. D. King-Smith, D. Vanderbilt, *Phys. Rev. B* **1993**, *47*, 1651.
[31] R. D. King-Smith, D. Vanderbilt, *Phys. Rev. B* **1994**, *49*, 5828.
[32] P. Ghosez, J.-P. Michenaud, X. Gonze, *Phys. Rev. B* **1998**, *58*, 6224.
[33] W. Tang, E. Sanville, G. Henkelman, *J. Phys.: Condens. Matter* **2009**, *21*, 084204.

[34] Z. Chen, X. Zou, W. Ren, L. You, C. Huang, Y. Yang, P. Yang, J. Wang, T. Sritharan, L. Bellaiche, L. Chen, *Phys. Rev. B* **2012**, *86*, 235125.

[35] Y.-M. Kim, A. N. Morozovska, E. A. Eliseev, A. R. Lupini, Y.-H. Chu, P. Yu, R. Ramesh, S. J. Pennycook, S. V. Kalinin, A. Y. Borisevich, *Microsc. Microanal.* **2013**, *19*, 1928.

[36] R. Guo, L. E. Cross, S.-E. Park, B. Noheda, D. E. Cox, G. Shirane, *Phys. Rev. Lett.* **2000**, *84*, 5423.

[37] Z. Fan, J. Xiao, H. Liu, P. Yang, Q. Ke, W. Ji, K. Yao, K. P. Ong, K. Zeng, J. Wang, *ACS Appl. Mater. Interfaces* **2015**, *7*, 2648.

[38] K. Ishikawa, T. Uemori, *Phys. Rev. B* **1999**, *60*, 11841.

[39] S. Tinte, M. G. Stachiotti, *Phys. Rev. B* **2001**, *64*, 235403.

[40] A. M. Bratkovsky, A. P. Levanyuk, *Phys. Rev. Lett.* **2005**, *94*, 107601.

[41] R. V. Wang, D. D. Fong, F. Jiang, M. J. Highland, P. H. Fuoss, C. Thompson, A. M. Kolpak, J. A. Eastman, S. K. Streiffer, A. M. Rappe, G. B. Stephenson, *Phys. Rev. Lett.* **2009**, *102*, 047601.